Anisotropic vortex-flux rotation in grain-oriented $YBa_2Cu_3O_7$

Liwen Liu and J. S. Kouvel
Department of Physics, University of Illinois at Chicago, Chicago, Illinois 60680

T. O. Brun
LANSCE, Los Alamos National Laboratory, Los Alamos, New Mexico 87545
(Received 16 April 1992)

Magnetization-vector measurements were made at 4.2 K on a grain-oriented $YBa_2Cu_3O_7$ sample rotated in the fixed external field $\mathbf{H}_e$ that was initially applied in the *a-b* plane or along the *c* axis during cooling from above T_c. The penetrating vortex-flux component of the sample magnetization was determined as a vector ($\mathbf{M}_P$) over a complete rotational cycle, with diamagnetic shielding and demagnetization effects taken into account. At low H_e, $\mathbf{M}_P$ turns rigidly with the rotating sample, and this simple behavior persists up to $H_e = 1$ kOe when applied along *c* during cooling. However, for $H_e = 1$ kOe applied along *a-b* during cooling, $\mathbf{M}_P$ reverses its direction in the *a-b* plane periodically, while its magnitude varies roughly as the projection of $\mathbf{H}_e$ on *a-b*. At higher H_e (≥ 3 kOe), the rotational behavior of $\mathbf{M}_P$ is the same for both field-cooling directions. One part of $\mathbf{M}_P$ continues to show a periodic vortex motion in and out of the *a-b* plane, while another part stays fixed in direction relative to $\mathbf{H}_e$ and thus turns frictionally relative to the rotating sample. The observed properties testify to a pronounced anisotropy of the vortex pinning forces, but many of their detailed features, including those that reveal a vortex cross-flux effect, are not yet clearly understood.

I. INTRODUCTION

One of the many intriguing aspects of the superconductivity of the CuO_2-layered compounds is the strongly anisotropic nature of the vortex state, as it reflects the pronounced crystallographic and electronic asymmetry. Experiments on crystals of prototypal $YBa_2Cu_3O_7$ have revealed[1,2] (as anticipated theoretically[3,4]) that the vortex lines are very different in morphology and in the strength of their pinning, depending on whether they are aligned along the crystal *c* axis or in the *a-b* plane. Consistent with an anisotropic vortex pinning, magnetic measurements on field-cooled crystals of $YBa_2Cu_3O_7$ and $Bi_2Sr_2CaCu_2O_8$ have shown[5] that, for different directions of the field applied during cooling, the trapped vortex flux is always oriented nearly parallel to the *c* axis. Although the latter results may be influenced by the highly anisotropic demagnetization of the thin-platelet samples,[6,7] they have subsequently been confirmed (but with a weaker *c*-axis preference) by our own trapped-flux measurements on a grain-oriented $YBa_2Cu_3O_7$ sample, in which the demagnetization of the crystallites is much less anisotropic.[8]

Our measurements on grain-oriented $YBa_2Cu_3O_7$ at 4.2 K also were carried out in external fields ($\mathbf{H}_e$) of various orientations, and the sample magnetization was determined as a vector $\mathbf{M}$, which could then be decomposed into its diamagnetic (shielding) and penetrating (vortex-flux) components, $\mathbf{M}_D$ and $\mathbf{M}_P$.[8] Thus, we were able to study $\mathbf{M}_P$ as it evolves with increasing H_e after zero-field cooling, and we found that it emerges (just above H_{cl}) as a vector much closer to the *a-b* plane, compared to the demagnetization-corrected field $\mathbf{H}$. This strong initial preference of the vortex-flux magnetization for the *a-b* plane is clear evidence that the vortex pinning is much weaker along *a-b* than along *c*.

Moreover, our magnetization-vector data on grain-oriented $YBa_2Cu_3O_7$ for all fields above H_{cl} revealed that $\mathbf{M}_P$ obeys an orientational scaling, in that its components along *a-b* and *c* plotted versus the corresponding components of the internal field $\mathbf{H}$ describe two universal curves.[8] The difference between these two curves gives a measure of the anisotropy of the vortex pinning forces, and the scaling itself has interesting implications concerning the crystallographic paths of the vortex lines. However, the scaling of the $\mathbf{M}_P$ components produced simultaneously by the components of $\mathbf{H}$ after zero-field cooling is curiously separate from the vortex cross-flux effect, in which we have observed that a trapped flux along *c* inhibits the subsequent production of vortex lines by a field along *a-b*.[9]

Our study of this cross-flux effect had originally been inspired by the suggestive results of some preliminary rotational experiments. These experiments, in which magnetization-vector measurements are made on a field-cooled grain-oriented sample of $YBa_2Cu_3O_7$, while it is slowly rotated in a fixed external field, have now been completed, and our results are presented in this paper. For various fields applied along *a-b* or along *c* during cooling, our findings include not only an anisotropic vortex pinning and a cross-flux effect but also a peculiar rotational behavior of vortex lines that lie weakly pinned in the *a-b* plane. Demagnetization effects, as calculated, introduce some complications but do not obscure the main features of our results.

II. EXPERIMENTAL DETAILS

As described previously,[8,9] our grain-oriented sample of $YBa_2Cu_3O_7$ was a circular disk (5 mm diameter, 1 mm thick) with the coaligned c axes of the crystallites (in an epoxy matrix) lying in the disk plane; the a and b axes are presumed to be randomly oriented in the normal basal plane. The sample was placed in a vibrating-sample magnetometer, where it could be rotated about its vertical disk axis in a fixed horizontal external field $\mathbf{H}_e$. By means of two sets of pickup coils mounted in quadrature, measurements were made of M_L and M_T, the longitudinal and transverse components of the sample magnetization relative to $\mathbf{H}_e$ in the disk plane.

The data reduction required dependable knowledge of the demagnetization effects. As a reasonable approximation, we assumed that the oriented crystallites in our sample have identical spheroidal shapes with their axes of rotation parallel to c, from which it follows (in cgs units) that

$$2D_{ab}+D_c=4\pi\ , \tag{1}$$

where D_{ab} and D_c are the demagnetization factors for $\mathbf{H}_e$ applied along a-b and c, respectively. It was also assumed that the diamagnetic shielding in our sample below H_{cl} is perfect in all directions, such that the magnetization $M=-H/4\pi$, where the internal field $H=H_e-DM$. Finally, since $M=m/V$, where m is the total magnetic moment and V is the collective volume of all the crystallites, these considerations combine to give

$$m_{ab}=-H_e^{(ab)}V/(4\pi-D_{ab}) \tag{2a}$$

and

$$m_c=-H_e^{(c)}V/(4\pi-D_c) \tag{2b}$$

for the measured moment along a-b or c as a linear function of the correspondingly directed external field.

By applying Eqs. (2a) and (2b) to our raw data for the initial susceptibilities along a-b and c (after zero-field cooling) and by invoking Eq. (1), we determined that $D_{ab}=3.36$ and $D_c=5.84$ (in Oe-cm^3/emu) and that $V=9.76\times10^{-4}$ cm^3. The values of D_{ab} and D_c imply that the spheroidal shape assumed for the crystallites is distinctly oblate, the dimension along c being about one half of the dimension in the a-b plane. (This dimensional ratio is typically much smaller in bulk crystals of $YBa_2Cu_3O_7$ grown by standard techniques, and the demagnetization is correspondingly much more anisotropic, i.e., $D_c\gg D_{ab}$.) The above value of V, when compared to the bulk volume of our sample disk (~0.02 cm^3), gives ~0.05 for the volume fraction of the crystallites, corresponding to a fairly dilute dispersion in the epoxy matrix.

We have used the value of V throughout in converting the measured magnetic moments into magnetizations. The values of D_{ab} and D_c were used separately, together with the experimental values for M_L and M_T, in determining H_{ab} and H_c, the components of the internal field $\mathbf{H}$ along a-b and c. For the external field $\mathbf{H}_e$ at angle θ_e relative to a-b, as shown in Fig. 1 (where both M_L and M_T are negative), the components of $\mathbf{H}$ are expressible as follows:

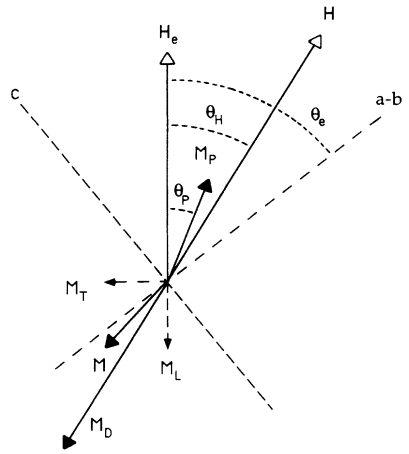

FIG. 1. Vector diagram showing external field $\mathbf{H}_e$, internal field $\mathbf{H}$, and total sample magnetization $\mathbf{M}$, composed of $\mathbf{M}_P$ and $\mathbf{M}_D$, its penetrating and diamagnetic components, relative to a-b plane and c axis. Also shown are $\mathbf{M}_L$ and $\mathbf{M}_T$, the measured longitudinal and transverse components of $\mathbf{M}$.

$$H_{ab}=(H_e-D_{ab}M_L)\cos\theta_e-D_{ab}M_T\sin\theta_e\ , \tag{3a}$$

$$H_c=(H_e-D_cM_L)\sin\theta_e+D_cM_T\cos\theta_e\ . \tag{3b}$$

The sample magnetization $\mathbf{M}$ was then decomposed into its diamagnetic and penetrating-vortex components, $\mathbf{M}_D$ and $\mathbf{M}_P$. Drawing upon our earlier findings for polycrystalline $YBa_2Cu_3O_7$,[10] we considered that $\mathbf{M}_D$ follows the initial susceptibility line (corrected for demagnetization) even at fields well above H_{cl}. Hence, consistence with our original assumption of perfect diamagnetic shielding in the grain-oriented sample, $\mathbf{M}_D=-\mathbf{H}/4\pi$, so that the vortex-flux magnetization $\mathbf{M}_P=\mathbf{M}+\mathbf{H}/4\pi$, whose components along a-b and c can be expressed as follows:

$$M_P^{(ab)}=M_L\cos\theta_e+M_T\sin\theta_e+H_{ab}/4\pi\ , \tag{4a}$$

$$M_P^{(c)}=M_L\sin\theta_e-M_T\cos\theta_e+H_c/4\pi\ , \tag{4b}$$

where H_{ab} and H_c are given by Eqs. (3a) and (3b). Thus, by inserting the measured M_L and M_T, the parameters D_{ab} and D_c, and the set variables H_e and θ_e into Eqs. (3a)–(4b), we have evaluated the a-b and c components of $\mathbf{H}$ and $\mathbf{M}_P$, from which we have determined their vector amplitudes and their orientational angles (θ_H and θ_P) relative to $\mathbf{H}_e$, as represented in Fig. 1.

III. RESULTS AND DISCUSSION

In each experiment, the grain-oriented $YBa_2Cu_3O_7$ sample was cooled from above T_c to 4.2 K in an external field $\mathbf{H}_e$ applied along a-b or c ($\theta_e=0°$ or 90° in Fig. 1). With H_e maintained at the same value, magnetization-vector data were taken, while the sample was rotated in steps up to $\theta_e\approx360°$ and back to $\theta_e=0°$. Our results for $H_e=0.3$ kOe applied along a-b during cooling are

displayed in Fig. 2, where the magnitude of the vortex-flux magnetization $\mathbf{M}_P$ and its orientational angle θ_P relative to $\mathbf{H}_e$ are plotted versus θ_e over the entire rotational cycle. We see that M_P initially descends to a shallow minimum near $\theta_e = 180°$ and then undulates gently through this minimum, whereas θ_P stays closely and reversibly equal to θ_e. Thus, despite its variations in magnitude, $\mathbf{M}_P$ remains oriented in the *a-b* plane and rotates rigidly with the sample. During this cycle, the calculated changes in the internal field are minor and have little effect on the behavior of $\mathbf{M}_P$.

For higher fields applied along *a-b* during cooling, the behavior of $\mathbf{M}_P$ rapidly becomes more complicated. Its magnitude develops a second minimum and both minima deepen, and at these values of θ_e the direction of $\mathbf{M}_P$ in the *a-b* plane reverses. The evolution of these changes is essentially complete when H_e reaches 1 kOe, for which our results for M_P and θ_p over a rotational cycle in θ_e are presented in Fig. 3. We see that both M_P and θ_P have taken on a remarkable periodic mode of behavior. During the forward and reverse rotations, M_P goes to nearly zero at θ_e hysteretically above or below 90° and 270°. At these θ_e values, θ_P switches almost abruptly by 180°, passing between linear variations in which θ_P equals θ_e, $\theta_e - 180°$, or $\theta_e - 360°$, as shown in the figure. Thus, $\mathbf{M}_P$ always lies in the *a-b* plane but goes through zero and reverses direction when its projection on $\mathbf{H}_e$ becomes slightly negative during the sample rotation. Whatever the mechanism may be for the changes in magnitude of $\mathbf{M}_P$, it is clear that the vortex lines in the *a-b* plane are so weakly pinned that they enter and exit the rotating sample very freely. Moreover, the confinement of the vortex lines to the *a-b* plane must reflect the strong pinning along the *c* axis.

Our data analysis for the latter experiment also yielded the magnitude of the internal field $\mathbf{H}$ and its orientational angle θ_H relative to $\mathbf{H}_e$. These quantities are plotted versus θ_e in Fig. 4, where they both exhibit sizeable systematic variations that primarily reflect the anisotropic demagnetization. Thus, in actual fact, the sample is not being rotated in a field of fixed size and direction. However, it appears very unlikely that the variations of H and θ_H have affected the extraordinary character of the changes of M_P and θ_P in Fig. 3. The implications of these changes therefore remain unaltered.

For $\mathbf{H}_e$ applied along the *c* axis during cooling, our results over the same range of fields ($H_e \leq 1$ kOe) are much simpler in that $\mathbf{M}_P$ stays along *c* with no reversals in direction as it turns rigidly with the sample. As shown in Fig. 5 for $H_e = 1$ kOe, this rigid rotational behavior is evidenced by the fact that θ_P, the angle between $\mathbf{M}_P$ and $\mathbf{H}_e$, varies very nearly as $\theta_e - 90°$, where $\theta_e = 90°$ corresponds to $\mathbf{H}_e$ being along *c*. Figure 5 also shows that $\mathbf{M}_P$ decreases in magnitude during the forward rotation and then remains fairly constant during the reverse rotation. Thus, apart from an initial adjustment in concentration, the vortex-flux lines produced by field cooling along *c* are held fairly along this axis by strong pinning forces. The magnitude of the internal field $\mathbf{H}$ and its orientational an-

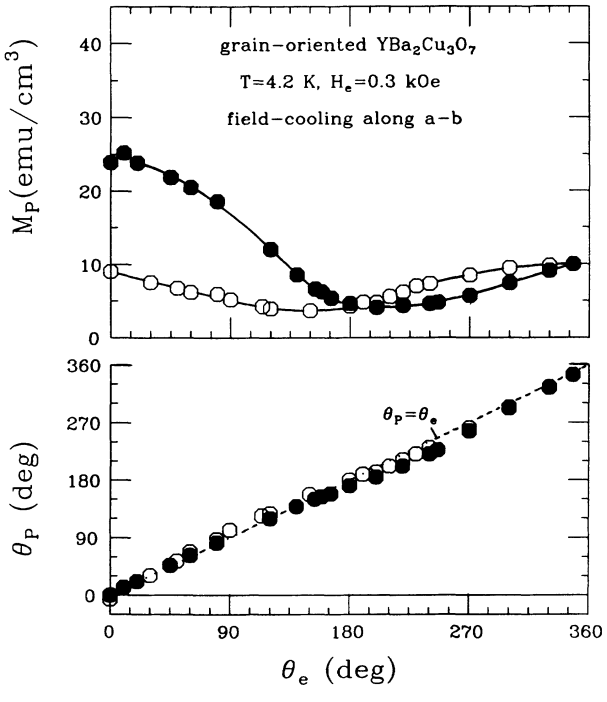

FIG. 2. Magnitude M_P and orientational angle θ_P of vortex-flux magnetization plotted vs sample-rotation angle θ_e for $H_e = 0.3$ kOe, initially applied along *a-b* ($\theta_e = 0°$) during cooling. Closed and open circles are for increasing and decreasing θ_e, respectively.

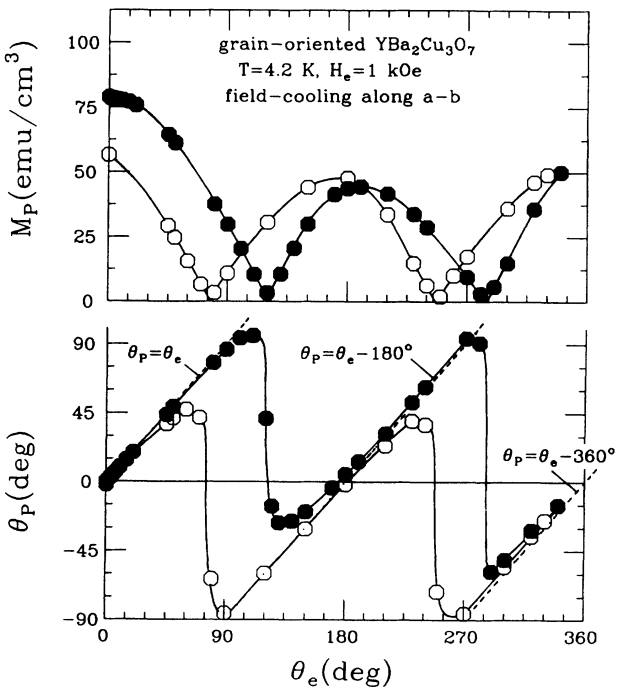

FIG. 3. Magnitude M_P and orientational angle θ_P of vortex-flux magnetization plotted vs sample-rotation angle θ_e for $H_e = 1$ kOe, initially applied along *a-b* ($\theta_e = 0°$) during cooling. Closed and open circles are for increasing and decreasing θ_e, respectively.

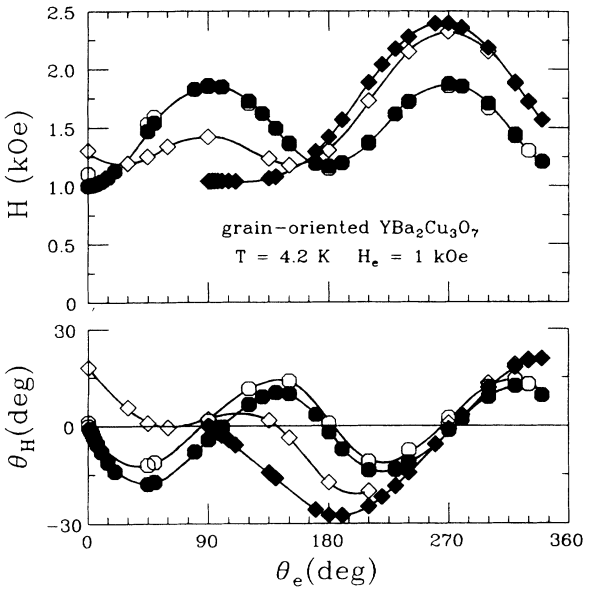

FIG. 4. Magnitude H and orientational angle θ_H of internal field plotted vs sample-rotation angle θ_e for $H_e=1$ kOe, initially applied along a-b (circles) or along c (diamonds) during cooling. Closed and open symbols are for increasing and decreasing θ_e, respectively.

gle θ_H are plotted versus θ_e in Fig. 4. Again, the variations are quite sizeable but do not seem to have affected the qualitative nature of the behavior of $\mathbf{M}_P$.

Although the variations of M_P and θ_P at $H_e=1$ kOe are strikingly different for field cooling along a-b and along c (Figs. 3 and 5), the behavior in the two cases changes and eventually merges at higher H_e. The merged behavior is exemplified by our results at $H_e=3$ kOe, which are displayed in Fig. 6. For both field-cooling directions (a-b and c), the magnitude of $\mathbf{M}_P$ undergoes an initial decrease and then settles into the same periodic variation in which it is maximum at $\theta_e=0°$, 180°, and 360°, where $\mathbf{H}_e$ is directed along a-b. Its orientational angle θ_P also shows a periodic variation in the two cases, but with a pronounced hysteresis such that the average θ_P is equal but opposite in sign for the forward and reverse directions of rotation. This rotational hysteresis testifies that some large part of $\mathbf{M}_P$ is turning frictionally relative to the sample. Thus, the 3 kOe field is large enough to overcome the strong vortex pinning to the crystal lattice. The sequential unpinning and repinning of the vortices in the rotating sample presumably occurs in abrupt steps and, therefore, is dissipative.

The peculiarities of the variations of M_P and θ_P in Figs. 3 and 6 suggested that additional clarification about the rotational changes might be gained from polar plots of the $\mathbf{M}_P$ vector in the fixed $\mathbf{H}_e$ frame. Accordingly, in Fig. 7, for the cases of $H_e=1$ and 3 kOe applied along a-b during cooling, we have plotted $M_P^{(L)}$, the longitudinal component of $\mathbf{M}_P$ (parallel to $\mathbf{H}_e$), against $M_P^{(T)}$, its transverse component (normal to $\mathbf{H}_e$), for different sample-rotation angles (θ_e). The plotted points, which are labeled at 90° intervals of θ_e (and at maximum $\theta_e=340°$),

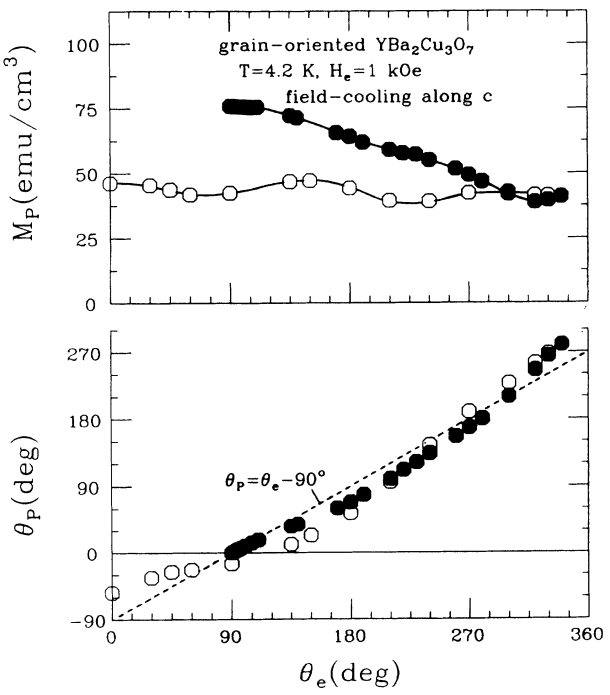

FIG. 5. Magnitude M_P and orientational angle θ_P of vortex-flux magnetization plotted vs sample-rotation angle θ_e for $H_e=1$ kOe, initially applied along c ($\theta_e=90°$) during cooling. Closed and open circles are for increasing and decreasing θ_e, respectively.

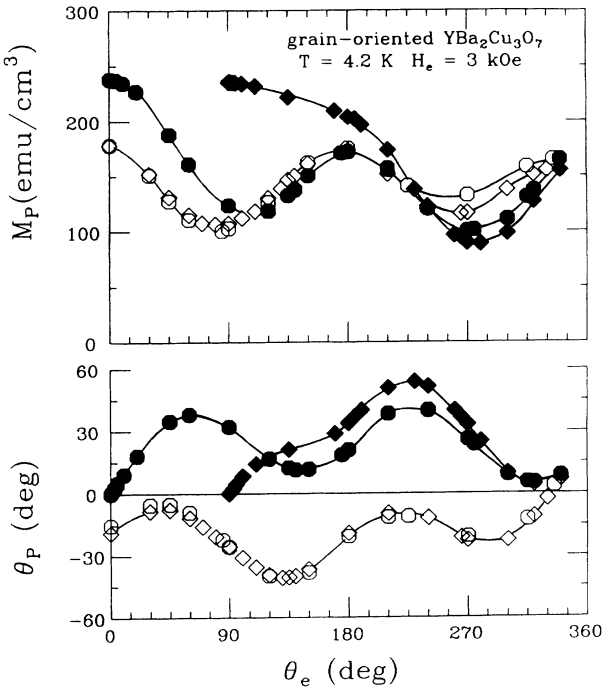

FIG. 6. Magnitude M_P and orientational angle θ_P of vortex-flux magnetization plotted vs sample-rotation angle θ_e for $H_e=3$ kOe, initially applied along a-b (circles) or along c (diamonds) during cooling. Closed and open symbols are for increasing and decreasing θ_e, respectively.

represent the ends of $\mathbf{M}_P$ vectors emanating from the origin.

For $H_e=1$ kOe, Fig. 7(a) reveals that the 180° periodicity in the magnitude of $\mathbf{M}_P$ as a function of θ_e is associated with a nearly circular steady-state variation in the polar plot. Specifically, the longitudinal and transverse components of $\mathbf{M}_P$ are seen to be varying approximately as

$$M_P^{(L)}=\tfrac{1}{2}M_0(1+\cos 2\theta_e) \tag{5a}$$

and

$$M_P^{(T)}=\tfrac{1}{2}M_0\sin 2\theta_e+M_h^{(T)}\ , \tag{5b}$$

where $M_0\approx 45$ emu/cm^3 and $M_h^{(T)}$ is a small hysteretic component ($\sim\pm 8$ emu/cm^3), which is positive (negative) for the forward (reverse) rotation of the sample. Transforming to the components of $\mathbf{M}_P$ along a-b and c, we find that if $M_h^{(T)}$ is ignored

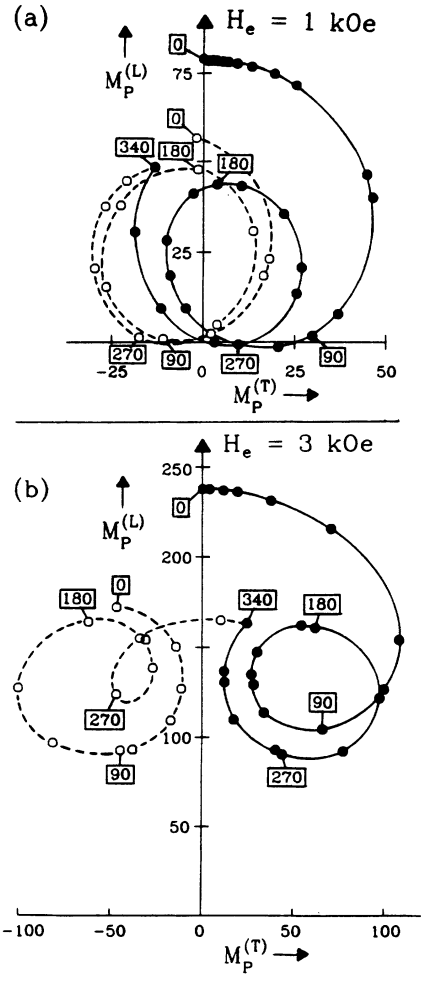

FIG. 7. Longitudinal and transverse components (relative to fixed $\mathbf{H}_e$) of vortex-flux magnetization, $M_P^{(L)}$ and $M_P^{(T)}$ (in emu/cm^3), plotted vs each other for (a) $H_e=1$ kOe and (b) $H_e=3$ kOe, initially applied along a-b during cooling. Closed and open circles are for increasing and decreasing sample-rotation angle θ_e, respectively, labeled at 90° intervals and at $\theta_e(\max)=340°$.

$$M_P^{(ab)}=M_P^{(L)}\cos\theta_e+M_P^{(T)}\sin\theta_e=M_0\cos\theta_e$$

and

$$M_P^{(c)}=M_P^{(L)}\sin\theta_e-M_P^{(T)}\cos\theta_e=0\ .$$

Thus, apart from its hysteretic component, the vortex-flux magnetization $\mathbf{M}_P$ lies in the rotating a-b plane and its magnitude is proportional to its projection on the stationary field $\mathbf{H}_e$.

Figure 7(b) shows that this peculiar steady-state rotational behavior of $\mathbf{M}_P$ persists at $H_e=3$ kOe; in fact, M_0 has grown to ~ 80 emu/cm^3. However, at this higher field, the hysteretic component displays an even greater relative increase. Its transverse part $M_h^{(T)}$ is now $\sim\pm 60$ emu/cm^3, and there is also a sizeable longitudinal part $M_h^{(L)}$ (~ 90 emu/cm^3), which should be added to the right-hand side of Eq. (5a). For each direction of rotation, the pronounced hysteretic component of $\mathbf{M}_P$ is clearly maintaining a fixed orientation relative to $\mathbf{H}_e$ by turning frictionally relative to the rotating sample. Hence, with regard to this component, the torque exerted on the vortex lines by $\mathbf{H}_e$ has overcome the restraining pinning torques. What then is remarkable is the coexistence of vortex lines that continue to lie in the a-b plane with a concentration that varies with their orientation relative to $\mathbf{H}_e$.

Since vortex lines appear to move easily in and out of the grain-oriented sample within the a-b plane, there seems to be an inconsistency with regard to the results in Fig. 5 for the case of $H_e=1$ kOe applied along the c axis during cooling. The figure shows essentially no periodic variation of M_P that would signal the entry of additional vortices whenever $\mathbf{H}_e$ becomes directed along a-b. Thus, it appears that the vortex lines that are trapped along the c axis and rotate rigidly with the sample inhibit the subsequent production of vortices in the a-b plane. This vortex cross-flux effect was originally detected in our preliminary rotational experiments and later documented in detail.[9] Interestingly, our present findings at the higher field of 3 kOe (Fig. 6) indicate that when the vortex pinning is ultimately overcome, vortices can again enter and exit freely in the a-b plane. These phenomena clearly follow a systematic pattern, which calls for a unified explanation.

In a very recent related study,[11] a combination of magnetization and magnetomechanical torque measurements was used to determine the magnetization vector $\mathbf{M}$ of stationary superconducting samples subjected to a cycled external field. The $\mathbf{M}$ vector was then decomposed into a reversible part arising from screening currents near the sample surface and an irreversible part associated with pinned vortices and screening currents throughout the sample. In the work reported here and previously,[10] our rotating-sample technique has enabled us to decompose $\mathbf{M}$ into a diamagnetic screening component, which is entirely reversible (even well above H_{c1}), and a penetrating vortex-flux component, which may contain both irreversible and reversible parts, the latter consisting of vortex flux that rotates rigidly with the sample, as exemplified in Fig. 2. Thus, the two decompositions are not equivalent and can lead to different conclusions.

ACKNOWLEDGMENTS

We are grateful for the theoretical interest of V. G. Kogan. The work at the University of Illinois at Chicago has been supported in part by the National Science Foundation under Grant Nos. DMR-87-22880 and DMR-90-24416. At the Los Alamos National Laboratory, support was provided by the U.S. Department of Energy under Contract No. W-7405-ENG-36 with the University of California.

[1]G. J. Dolan, G.V. Chandrashekhar, T. R. Dinger, C. Feild, and F. Holtzberg, Phys. Rev. Lett. **62**, 827 (1989); G. J. Dolan, F. Holtzberg, C. Feild, and T. R. Dinger, *ibid.* **62**, 2184 (1989).

[2]W. K. Kwok, U. Welp, V. M. Vinokur, S. Fleshler, J. Downey, and G. W. Crabtree, Phys. Rev. Lett. **67**, 390 (1991).

[3]L. J. Campbell, M. M. Doria, and V. G. Kogan, Phys. Rev. B **38**, 2439 (1988); V. G. Kogan and L. J. Campbell, Phys. Rev. Lett. **62**, 1552 (1989).

[4]M. Tachiki and S. Takahashi, Physica C **162-164**, 241 (1989); Solid State Commun. **70**, 291 (1989).

[5]I. Felner, U. Yaron, Y. Yeshurun, G. V. Chandrashekhar, and F. Holtzberg, Physica C **162-164**, 1635 (1989); Phys. Rev. B **40**, 5239 (1989).

[6]S. Kolesnik, T. Skoskiewicz, and J. Igalson, Phys. Rev. B **43**, 13 679 (1991).

[7]I. Felner, U. Yaron, and Y. Yeshurun, Phys. Rev. B **43**, 13 681 (1991).

[8]Liwen Liu, J. S. Kouvel, and T. O. Brun, Phys. Rev. B **45**, 3054 (1992).

[9]Liwen Liu, J. S. Kouvel, and T. O. Brun, Phys. Rev. B **43**, 11 481 (1991).

[10]Liwen Liu, J. S. Kouvel, and T. O. Brun, J. Appl. Phys. **67**, 4527 (1990); Phys. Rev. B **43**, 7859 (1991); J. Appl. Phys. **70**, 5733 (1991).

[11]F. Hellman, E. M. Gyorgy, and R. C. Dynes, Phys. Rev. Lett. **68**, 867 (1992).